RSC Advances

ROYAL SOCIETY OF CHEMISTRY

www.rsc.org/advances

Micellar self-assembly, bridging and gelling behaviour of two reverse triblock poly(butylene oxide)-poly(ethylene oxide)-poly(butylene oxide) copolymers with lengthy hydrophilic blocks.

Adriana Cambón,[a⊥] Edgar Figueroa-Ochoa,[b⊥] Mateo Blanco,[a] Silvia Barbosa,[*a] José Félix Armando Soltero,[b] Pablo Taboada,[a] Víctor Mosquera[a]

[a]*Grupo de Física de Coloides y Polímeros, Departamento de Física de la Materia Condensada; 15782-Santiago de Compostela, Spain.*
[b]*Laboratorio de Reología, Departamento de Ingeniería Química, CUECI, Universidad de Guadalajara, Blv. M. García Barragán 44430, Jalisco, México.*

[*]Author to whom correspondence should be addressed: silvia.barbosa@usc.es

[⊥]These authors contribute equally to this work

Abstract

Triblock polyethyelene oxide-polybutylene oxide-based block copolymers overcome some of the synthetic drawbacks of commercially available Pluronic block copolymers as well as providing a more hydrophobic environment to solubilise poorly aqueous-soluble compounds. These facts can be exploit to use this class of copolymers as efficient drug delivery nanocarriers (A. Cambón et al. Int. J. Pharm. 2013, 445, 47-57), and their interactions with biological relevant entities and biological performance should be regulated by the nature, conformation and state of the copolymeric chains. For this reason, in this work we investigated the self-assembly process of two of these reverse triblock poly(butylene oxide)-poly(ethylene oxide)-poly(butylene oxide) block copolymers, $BO_8EO_{90}BO_8$ and $BO_{20}EO_{411}BO_{20}$, to obtain a clear picture of their self-assembly behaviour in order to correlate it with their biological performance. As a consequence of their particular structure, $BO_{20}EO_{411}BO_{20}$ possess a rich rheological behavior characterized by the formation of flower-like micelles (ca. 10 to 30 nm in size) and intermicellar bridging at low copolymers concentrations, as denoted by atomic force microscopy and rheology data. Conversely, $BO_8EO_{90}BO_8$ displays a behaviour more similar as that observed for diblock EO_mBO_m and direct triblock $EO_mBO_nEO_n$ copolymers, with single non-associated micelles at low concentrations, and a flow behaviour typical of mesoscopic ordered cubic structures. Strikingly, the relatively wide Poisson distribution of the copolymeric chains makes the present copolymers to behave also rather distinctly to conventional associative thickeners.

Introduction

Hydrophobically end-capped poly(oxyethylene oxide)s have applications in paint coatings, personal care products and in the oil industry because of their ability to dramatically modify rheological properties.[1-4] The industrially important type are the HEUR (hydrophobically ethoxylated urethane) associating polymers, which comprise lengthy poly(oxyethylene) chains end-capped via urethane links by alkyl chains. Corresponding poly(oxyethylene) dialkyl ethers and esters have been also used.[5-6] Their desirable properties originate from molecular association of the hydrophobic ends of the chains in dilute solution and, above a critical micelle concentration (cmc), from the association of molecules into micelles in which the chains can either loop or extent.[7] The bridging of chains between micelles, a dynamic process, leads to the formation of transient micelle clusters and networks.

Conventional triblock copolymers with hydrophobic end blocks, in particular triblock poly(oxyalkylene)s, offer a different synthetic route with the potential for interesting differences in properties and potential applications, as reported for $PO_nEO_mPO_n$,[8-9] $BO_nEO_mBO_n$[10-13] and $SO_nEO_mSO_n$,[14-15] where EO, PO, BO and SO denote ethylene oxide, propylene oxide, butylene oxide and styrene oxide blocks, respectively. Amongst them, $PO_nEO_mPO_n$ copolymers have been the most extensively studied due to their commercial availability in a range of compositions. However, these copolymers present several drawbacks as, for example, their inherent polydispersity after oxyanionic polymerization as a consequence of the transfer reaction from hydrogen abstraction during the polymerization of the PO blocks,[16] which results in an important diblock component in the synthesized material. This gives rise to variations in their physico-chemical properties from batch to batch which can preclude their use in different applications where an accurate reproducibility of the physico-chemical properties is required such as, for example, in drug delivery since these copolymers are amphiphilic and are able to self-assemble into nanoscopic core-shell micelles. The micellar core may serve as a reservoir for hydrophobic cargos while the corona provides stability and stealthiness into the aqueous biological medium.

An alternative to $PO_nEO_mPO_n$ copolymers is $BO_nEO_mBO_n$ ones provided that transfer is not a problem in the laboratory polymerization of butylene oxide and, hence, the chain distributions are much narrower. In addition, the larger relative hydrophobicity of BO blocks compared to PO (six-fold as estimated from the ratio of the logarithms of the cmcs)[17] allows the formation of polymeric micelles and of transient micelle clusters and/or networks by bridging of extended chains between micelles[13,18] at much lower concentrations than $PO_nEO_mPO_n$ do. This may enable their use as nanocarriers to solubilize much higher concentrations of poorly aqueous soluble drugs in a reproducible manner[19] in the form of injectable solutions, oral suspensions and/or sub-dermal gelling depots[19-21] provided that these copolymers have been proved to be biocompatible.[22] However, a detailed and complete characterization of the physico-chemical properties of this class of copolymers is still lacking: A deep knowledge about the correlations between copolymer structure and reflected properties must be key to explain, for example, the

biological activity of some of these copolymers, for example, as enhancers of drug toxicity to cancerous cells by inhibiting the P-glycoprotein P efflux pump mechanism, [19] which seems to be regulated by the nature, conformation and state of the copolymeric chains

Hence, in this work we analyze the physico-chemical behaviour in aqueous solution of two $BO_nEO_mBO_n$ block copolymers: $BO_8EO_{90}BO_8$ and $BO_{20}EO_{411}BO_{20}$, which largely differ in the hydrophilic block length. This should result in large differences in the micellization process, intermicellar interactions and, thus, solution behaviour. In particular, as a result of its long BO blocks and extremely lengthy EO ones copolymer $BO_{20}EO_{411}BO_{20}$ clearly shows the formation of micellar clusters formed by micellar bridging as observed from dynamic light scattering (DLS), atomic force microscopy (AFM), and rheometry. Due to their shorter EO and BO blocks, copolymer $BO_8EO_{90}BO_8$ behaves more similarly to a solution of interacting micelles, which pack in a mesoscopic structure (a gel) at large concentrations, although some extent of bridging could be also detected. The differences in the copolymer structures allows us then to observe the effects of both the collapse of longer BO blocks in solution of reverse copolymeric structures and the splitting of BO units number between two blocks, especially in dilute solution since the range of hydrophobicity has been much restricted for these copolymers *i.e.* from BO_4 to BO_{12}, 8 to 24 BO units per molecule.[17]

Materials and methods

Materials

Triblock copolymers were prepared by oxyanionic polymerisation as previously reported.[10] Briefly, dry 1,2-butylene oxide was initiated by polyethylene glycol monomer of different molecular weights activated by mixing with KOH and heating while stirring under vacuum (70 ºC, 0.1 mmHg, 100 h) to remove water. Vacuum line and ampoule techniques served to exclude moisture. Gel permeation chromatography (GPC) was used to characterize the distribution widths of the products as the ratio of mass-average to number-average molar mass, *i.e.* M_w/M_n by using a Waters GPC system equipped with a 1515 isocratic pump and a 2410 refractive index detector (Waters, Milford, MA). Chloroform was used as eluent, and monodisperse PEO was employed as standard. ^{13}C NMR spectra recorded on a Bruker ARX400 spectrometer (Bruker, Milton, ON, Canada) in deuterated chloroform were used to obtain absolute values of block length and composition, and to verify block architecture. Table 1 summarises the molecular characteristics of the copolymers.

Table 1. Molecular characteristics of the copolymers

Polymers	M_n	M_w/M_n [b]	M_w	*cmc*

	(g/mol)[a]		(g/mol)	(g/dm^3)[c]
$BO_8EO_{90}BO_8$	5100	1.07	5457	0.33
$BO_{20}EO_{411}BO_{20}$	21000	1.08	22680	0.01

[a]Estimated by NMR; [b]Estimated by GPC; M_w calculated from M_n and M_w/M_n. Estimated uncertainty: M_n to ±3 %; M_w/M_n to ±0.01.[c]Values from Ref. 10.

Dynamic and static light scattering (DLS and SLS)

SLS intensities were measured by means of an ALV-5000F (ALV-GmbH, Germany) instrument with vertically polarized incident light (λ = 488 nm) supplied by a diode-pumped Nd:YAG solid-state laser (Coherent Inc., CA, USA) and operated at 2 W, and combined with an ALV SP-86 digital correlator with a sampling time of 25 ns to 100 ms (for DLS). Measurements were made at an angle θ = 90° to the incident beam, as appropriate for particles smaller than the light wavelength. The intensity scale was calibrated against scattering from toluene. Solutions were filtered through Millipore Millex filters (Triton free, 0.22μm porosity) directly into cleaned scattering cells and allowed to equilibrate at the requested temperature for 10 min before measurement. Each experiment was repeated at least three times. Sampling time was 5-10 minfor each run in order to define an optimal correlation function.

To obtain the micellar molecular weights and aggregation number, Debye plots *i.e*. plots based on

$$\frac{K^* c}{I - I_S} = \frac{1}{M_w^m} + 2A_2 c + \cdots \qquad (1)$$

where I is the light scattering intensity from solution relative to that from toluene, I_S is the corresponding quantity for the solvent, c is the concentration (in g dm^{-3}), M_w^m is the mass-average molar mass of the solute, A_2 the second virial coefficient, and K^* the appropriate optical constant, were used. K^* includes the specific refractive index increment (dn/dc), whose insensitiveness to composition in $BO_nEO_mBO_n$ systems is already known (dn/dc = 0.135 cm^3/g).[23]

For DLS, the correlation functions were analyzed by the CONTIN method to obtain the intensity distributions of decay rates (Γ).[24] From the decay rate distributions the apparent diffusion coefficients ($D_{app} = \Gamma/q^2$, $q = (4\pi n_S/\lambda)\sin(\theta/2)$ were derived, being n_S the solvent refractive index. Values of the apparent hydrodynamic radius ($r_{h,app}$, radius of the hydrodynamically equivalent hard sphere corresponding to D_{app}) were calculated from the Stokes-Einstein equation

$$r_{h,app} = kT/(6\pi\eta D_{app}) \qquad (2)$$

where k is the Boltzmann constant and η is the viscosity of water.

Transmission electron microscopy (TEM)

Micellar solutions of both copolymers were applied dropped over carbon-coated copper grids, blotted, washed, negatively stained with 2% (w/v) phosphotungstic acid, air-dried, and then examined with a Phillips CM-12 transmission electron microscope operating at an accelerating voltage of 120 kV.

Clouding

Copolymer solutions were prepared by weighting the requested amount of each copolymer followed by the addition of the same volume of cold water (1 mL). Copolymer solutions were homogenized under stirring at low temperature before being stored at least for one day (T ~ 4 ºC) to ensure complete dissolution. Clouding temperatures (T_{cl}) were determined by slowly heating (0.2 ºC min^{-1}) the copolymer solutions from 0 to 90 ºC by both visual inspection and detection of the transmitted light through solutions by meansof a Cary Eclipse UV-Vis spectrophotometerequipped with a temperature control Peltier device and a multi-cell sample holder (Cary 100, Agilent, Germany). As a result, a plot of transmitted intensity versus temperature was obtained. The cloud point was determined as the midpoint of an abrupt decrease in the transmitted light intensity from a plot of transmitted intensity *vs* temperature, as previously described.[18]

Rheology

Solutions were prepared by weighting powder copolymer and deionized water into small tubes and subsequent mixing in the mobile state before being stored for at least one day at low temperature (ca. 4 ºC). Rheological characterisation was carried out using a controlled stress AR2000 rheometer (TA instruments, DE, USA) with Peltier temperature control. Samples were investigated using cone-plate geometry and a solvent trap to maintain a water-saturated atmosphere around the sample cell to avoid evaporation. The temperature dependence of storage (G) and loss (G'') moduli was measured either by temperature scans (1-90 ºC) at frequency f = 1 Hz and heating rates of 1 ºC min^{-1} or via frequency scans at several temperatures. Experiments were carried out in oscillatory shear mode, with the strain amplitude (A) maintained at a low value (A< 0.5 %) by means of the autostress facility of the software. This ensured that measurements of G' and G'' were in the linear viscoelastic region. A dynamic time sweep test under A = 0.5% and f = 1 Hz was performed before each frequency scan at a fixed temperature to ensure that the sample truly reached the equilibrium state.

Atomic force microscopy (AFM)

AFM images of block copolymer solutions were performed on freshly cleaved mica substrates. The measurements were performed in a JEOL instrument (model JSPM 4210) in noncontact mode using nitride cantileversNSC15 from MicroMasch, U.S.A. (typical working frequency and spring constant of 325 kHz and 40 N/m, respectively). The AFM samples were dried in air or under a nitrogen flow when required. Control samples (freshly cleaved mica and buffer solution) were also investigated to exclude possible artifacts. Topography and phase-shift data were collected

in the trace and retrace direction of the raster, respectively. The offset point was adapted accordingly to the roughness of the sample. The scan size was usually 500 nm (aspect ratio, 1 x 1), with a sample line of 256 points and a step size of 1 μm. The scan rate was tuned proportionally to the area scanned and kept within the 0.35-2 Hz range. Each sample was imaged several times at different locations on the substrate to ensure reproducibility. Diameters and heights of copolymer aggregates were determined by sectional analysis taken from the average of several sections through the aggregates.

Results and Discussion

Clouding

Clouding temperatures (T_{cl}) were firstly determined for solutions of copolymers $BO_8EO_{90}BO_8$ and $BO_{20}EO_{411}BO_{20}$ in the concentration range 0.1-10 wt.% by visual inspection and UV-Vis spectroscopy following the methodology of Zhou *et al*.[18] For $BO_8EO_{90}BO_8$ the cloud-point profile exhibited a shallow minimum at 0.75 wt.% (at 43 ºC), whilst for $BO_{20}EO_{411}BO_{20}$ this minimum was observed at 1.5 wt.% (at 41 ºC) (Figure 1). For both copolymers T_{cl} starts again to increase at larger concentrations from their respective minima. In general, copolymer $BO_8EO_{90}BO_8$ displayed lower T_{cl} than $BO_{20}EO_{411}BO_{20}$ as a consequence of their lower EO/BO ratio: Regardless copolymer $BO_{20}EO_{411}BO_{20}$ contains much longer BO blocks which should largely decrease T_{cl}, the extremely long hydrophilic EO block counterbalances this effect and favors an important enhancement of T_{cl}, [25] in agreement with previous observations.[11,26] This behavior is further supported when comparing, for example, copolymer $BO_8EO_{90}BO_8$ with the structurally related $BO_7EO_{40}BO_7$: By doubling the EO block length while keeping almost constant the BO one results in a great increase of T_{cl} from 35ºC to 75 ºC at a copolymer concentration of 10 wt.%[18]. In addition, an increase in the BO block length while keeping constant the EO one leads to an important decrease in T_{cl}, for example, from 53 to 41.5 ºC at 2 wt.% when comparing, for example, copolymers $BO_{10}EO_{410}BO_{20}$ and $BO_{20}EO_{411}BO_{20}$, or from 66 to 57ºC for copolymers $BO_{14}EO_{378}BO_{14}$ and $BO_{21}EO_{385}BO_{21}$, respectively.[27] However, it is worth mentioning that for concentrations above 3.5 wt.% the more efficient packing of $BO_{20}EO_{411}BO_{20}$ micelles and their subsequent packing and ordering in solution (gel formation) leads to a sharper T_{cl} increase above those values corresponding to copolymer$BO_{10}EO_{410}BO_{20}$ (Figure 1a). High T_{cl} coincident with gel formation have been also observed in related systems, *i.e.* aqueous solutions of copolymers $BO_{12}EO_{114}BO_{12}$ and $BO_{12}EO_{227}BO_{12}$.[12,13,28]

Provided that the *cmc* values of the present copolymers were previously found to be below 0.35 mg/mL (see Table 1),[10] the cloud point behavior would represent the phase transition of a copolymer micellar solution which phase separates at a temperature well above the T_{cl}. On the other hand, plotting T_{cl} values against EO/BO ratio at fixed copolymer concentration (1 wt.%) an empirical correlation for $BO_nEO_nBO_n$ copolymers with short (≤ 10) and long (≥ 10) BO blocks could be observed (Figure 1b). The lowest values of T_{cl} are directly dependent on copolymer hydrophobicity, that is, T_{cl} at the minimum decreases as the EO/BO ratio does (Table S1).

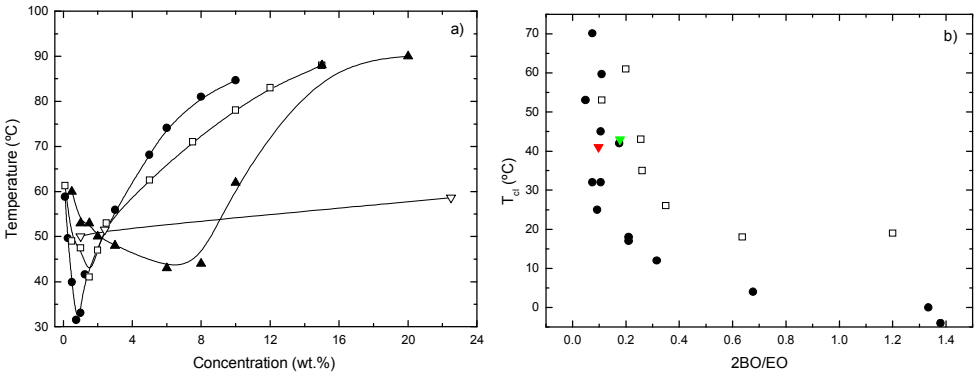

Figure 1. a) Clouding temperatures for $BO_nEO_mBO_n$ triblock copolymers as a function of concentration: (●) $BO_8EO_{90}BO_8$ and (□) $BO_{20}EO_{411}BO_{20}$. For comparison, structurally-related copolymers (▽) $BO_5EO_{91}BO_5$ and (▲) $BO_{10}EO_{410}BO_{10}$ (11) are also shown. b) Minimum clouding temperatures copolymers as a function of BO/EO block length ratio for $BO_nEO_mBO_n$ triblock with (□) BO < 10 and (●) BO > 10. The present $BO_8EO_{90}BO_8$ and $BO_{20}EO_{411}BO_{20}$ copolymers are shown in green and red, respectively.

Population size distributions

DLS measurements of micellar solutions of copolymers $BO_8EO_{90}BO_8$ and $BO_{20}EO_{411}BO_{20}$ at different concentrations were carried out at 10 and 25 °C. Selected intensity fraction distributions of log $r_{h,app}$ ($r_{h,app}$ being the apparent hydrodynamic radius, *e.g.* the radius of gyration of the hydrodynamically equivalent hard sphere) are illustrated in Figure 2a for copolymer $BO_8EO_{90}BO_8$ at 25 ºC as an example. At the lowest concentration analysed (0.1 wt. %), the population distribution showed a single peak attributed to flower-like micelles ($r_{h,app}$ ~ 13 nm). At larger concentrations (0.25 wt.%), two peaks were observed in the intensity-fraction population distributions,which can correspond to micelles and micelle clusters formed by micellar bridging ($r_{h,app}$= 140 nm), respectively. Further increases in copolymer concentration leads to an enhancement of the light scattered by flower-like micelles and to a certain reduction (in intensity) in the population distribution of the micellar clusters, which shifts to larger sizes and becomes broader (ca. 200 nm). This behaviour can be probably a consequence, on one hand, of a better packing of BO blocks inside micelles as the copolymer concentration increases and, on the other, to an extension of bridging resulting in associated larger micellar clusters.

Owing to the special chain architecture of $BO_nEO_mBO_n$-type block copolymers, the formation of flower-like micelles involves the bending of the hydrophilic EO blocks while keeping the two-end BO blocks in the same micellar core, which is an entropycally-loss process. Another possibility is that the two BO blocks in one polymer chain can reside in two adjacent micelles while the EO block is used as a bridge. This kind of cross-linking among the micelles can finally promote an open network structure (the so-called micellar clusters), which is reflected in the DLS population distributions.

Copolymer $BO_{20}EO_{411}BO_{20}$ possessed a similar behaviour as $BO_8EO_{90}BO_8$except that sizes of micelles and micellar clusters become larger due to the lengthy EO blocks of this copolymer. At this respect, it is worth

mentioning that micellar cluster sizes for this copolymer reaches ca. 900 nm, and even a third much larger population at ca. 3000-4000 nm can be observed probably being a result of the formation of insoluble aggregated material as a consequence of cluster aggregation (Figure 2a). For both $BO_8EO_{90}BO_8$ and $BO_{20}EO_{411}BO_{20}$the micellar shape was nearly spherical as observed by TEM and AFM, with their diameters (ca. 22 ± 4 and 32 ±5 nm for $BO_8EO_{90}BO_8$ and $BO_{20}EO_{411}BO_{20}$ as calculated from TEM, respectively), in fair agreement with those obtained from DLS in spite of the usual dehydration of the copolymer corona and subsequent shrinking of the copolymer structure upon solvent evaporation during sample preparation (Figure 2b). From AFM images a deformation of the EO corona can be observed as a result of bridging and subsequent formation of micellar clusters (Figure 2c).

Intensity-average values of $1/r_{h,app}$ were calculated for micelles by integrating over the micelles peak in the intensity distributions of decay rate. Since the dissymmetry ratio was found to be near unity, the values obtained were essentially *z*-averages. Micellar hydrodynamic radii (r_h) were obtained as the intercept of each curve at $c = 0$ (Figure 2e and Table 3) from plots of $1/r_{h,app}$ against copolymer concentration. $1/r_{h,app}$ is proportional to the apparent diffusion coefficient, D_{app}, but without the influence of temperature and solution viscosity. It can be observed that the average values of $r_{h,app}$ increased as concentration did, *i.e.* the apparent diffusion coefficient ($D_{app}= kT/ 6\pi\eta r_{h,app}$) decreased (Figure 2d). Also, micellar sizes become smaller as the temperature decreases. This was as expected provided that water becomes a better solvent for micelles as the temperature is lowered and, hence, micellar bridging (and hence clustering) was reduced.

The negative slopes of plots in Figure 2d and, hence, the negative second virial coefficients (A_2) derived as reported previously (Table 3, see SI for additional details)[29] implies a substantial attractive contribution to their intermicellar interaction, resulting in small excluded volumes for the micelles of $BO_nEO_mBO_n$ copolymers, especially for $BO_8EO_{90}BO_8$ due to its shorter EO corona which, in turn, results in small values of A_2. This is consistent with the micelles having a fraction of their BO blocks extended into the solvent and available for interaction, either with BO blocks protruding from a second micelle or by entering the core of a second micelle, as confirmed visually (Figure 2c-d), and considering that Van der Waals attraction and polymer depletion forces would not play significant roles in the present relatively dilute micellar systems.[18,23] In either case, the effect results in transient micellar linking, which implies a second equilibrium in the system:

$$N\mathrm{A} \leftrightarrow \mathrm{A}_N \text{ (molecule/micelle equilibrium)}$$

$$M\mathrm{A}_N \leftrightarrow (\mathrm{A}_N)_M \text{ (micelle/linked-micelles equilibrium)}$$

Both BO and EO block lengths will affect these interactions: Longer BO-end blocks imply that the intermicellar interaction can become stronger, while central EO blocks can make the BO blocks to be more or less extended into the solution.[30] The smaller (more negative) A_2 values for copolymer $BO_{20}EO_{411}BO_{20}$ compared to those

of $BO_8EO_{90}BO_8$ might be a consequence of the longer BO and EO blocks of the former copolymer which favoured direct contacts between micelles even at very low concentrations. Also, A_2 coefficients increases (become less negative) as temperature raises as a consequence of water becoming a worst solvent for micelles; this would make EO coronas to be less hydrated and shrunk, and it would decrease the extent of bridging in agreement with static light scattering data (see below).

In summary, the present data would support the view that for molecules of this type limited open molecular association accompanies closed association to micelles. This means (in a simplified model) that several components are in equilibrium: molecules, micelles, and micellar associates (bridged micelles).

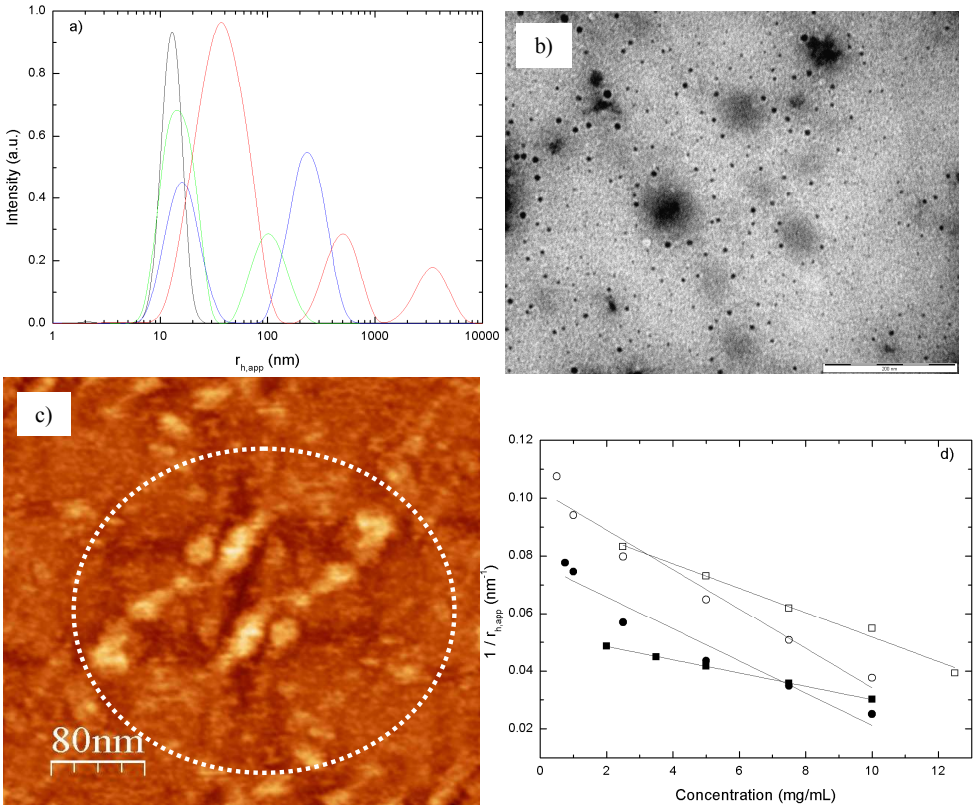

Figure 2. a) Intensity-weighted population distributions obtained by DLS for copolymer $BO_8EO_{90}BO_8$ in solution at 25ºC (black, green and blue lines correspond to 0.1, 0.5 and 1 wt.% solutions, respectively) and copolymer $BO_{20}EO_{411}BO_{20}$ (1 wt.%, red line). b) TEM image of $BO_{20}EO_{411}BO_{20}$ micelles at a concentration of 0.5 wt.% (scale bar 200 nm). c) AFM image of $BO_{20}EO_{411}BO_{20}$ copolymer showing interchain bridges between micelles. d) Reciprocal apparent hydrodynamic radius, $1/r_{h,app}$, against concentration for copolymers $BO_8EO_{90}BO_8$ (●,○) and $BO_{20}EO_{411}BO_{20}$ (■,□) in solution at 10 ºC (open symbols) and 25 ºC (filled symbols).

Micellar properties

Since the hydrodynamic radii of the present micelles (listed in Table 3) are small compared to the light wavelength, intraparticle interference can be neglected. Clustering at higher concentrations changes this picture, but we here focused on the behaviour in the dilute micellar regime. Debye plots for copolymers $BO_8EO_{90}BO_8$ and $BO_{20}EO_{411}BO_{20}$ at 10 and 25 ºC are shown in Figure 3. These plots indicate associates of higher molar mass at 25 ºC

compared with 10 ºC for both copolymers, as expected for water to be a poorer solvent at the highest temperature. The overall scattering behavior of $BO_8EO_{90}BO_8$ and $BO_{20}EO_{411}BO_{20}$ copolymer solutions is consistent with a closed association process into micelles, but the slopes and curvatures of the Debye plots at the highest concentrations (specially for copolymer $BO_{20}EO_{411}BO_{20}$) are much changed compared with those for EO_nBO_n or $EO_nBO_mEO_n$ copolymers. Although at low concentrations the present copolymers, and especially $BO_8EO_{90}BO_8$, tend to loop in isolated micelles there is a finite probability of bridging because the system is in dynamic equilibrium, which implies an attractive intermicellar interaction. Hence, the minima and low positive slopes seen in Figure 3b for $BO_{20}EO_{411}BO_{20}$ results from the competition between repulsive and attractive interactions between the micelles, which are less important for copolymer $BO_8EO_{90}BO_8$ at 25 ºC, in agreement with our interpretation of the DLS results in the former section. The repulsive interaction, effectively a hard-sphere interaction, clearly dominates at the largest concentrations where higher virial coefficients are required to describe the slope of the Debye plots. The effect of the attractive interaction between micelles, which derives from bridging, is seen at lower concentrations where A_2 dominates, and represented by the upturns in the plots for copolymer $BO_{20}EO_{411}BO_{20}$. In this case, such upturns cannot be ascribed to the micelle-molecule equilibrium, *i.e.* the dissociation of micelles at concentrations approaching the critical micelle concentration, provided that the concentration range analyzed is well above the copolymers *cmcs*.

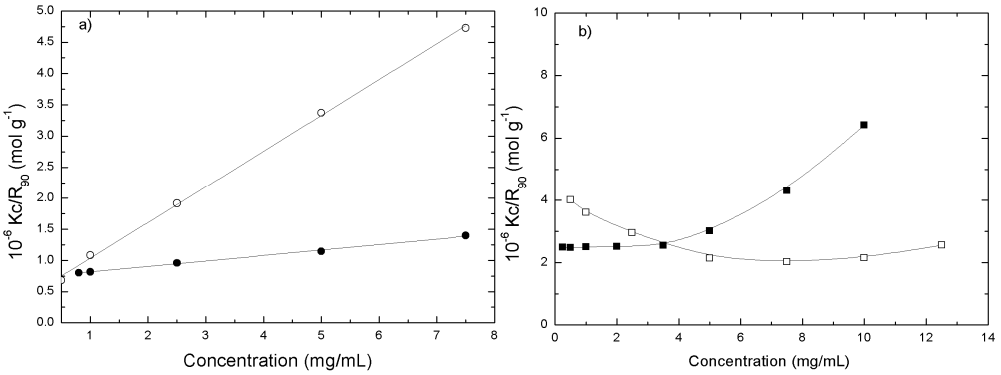

Figure 3. Debye plots for a) $BO_8EO_{90}BO_8$ and b) $BO_{20}EO_{411}BO_{20}$ copolymers at 10 ºC (open symbols) and 25 ºC (filled symbols).

Values of M_w^m were obtained by simply applying the Debye equation for copolymer $BO_8EO_{90}BO_8$ and by linear extrapolation of experimental data at c < 5 mg/mL and by for $BO_{20}EO_{411}BO_{20}$, respectively, and calculated from $N_w = M_w^m/M_w$ (Table 2). The almost ideal behavior of the $BO_8EO_{90}BO_8$ system at low concentration is attributed to counter-balanced attractive and repulsive interactions of micelles in the dilute solution range and the polymer ability to pack in single micelles at low concentrations due to its much shorter blocks, as commented previously (see Figure 2a).

Association numbers for copolymer $BO_8EO_{90}BO_8$ were larger than those of $BO_{20}EO_{411}BO_{20}$ as corresponds to a copolymer with a lower EO/BO ratio and much shorter EO block length: The increment of N_w due to the presence of longer BO blocks for copolymer $BO_{20}EO_{411}BO_{20}$ was counter-balanced by the N_w decrease expected by their longer EO blocks, as observed for other poly(oxyalkylene)s copolymers.[16] Also, N_w values for these copolymers

slightly increased as temperature rose provided that water becomes a poorer solvent for the poly(oxyethylene) blocks, as previously mentioned[17]. Association numbers of copolymer $BO_{20}EO_{411}BO_{20}$ are similar to those obtained for the structurally related copolymer $BO_{10}EO_{410}BO_{10}$ despite its larger BO block length, and are lower than those of other $BO_mEO_nBO_m$ with lengthy EO blocks such as $BO_{14}EO_{378}BO_{14}$ (N_w = 18),[29] $BO_{12}EO_{270}BO_{12}$ (N_w = 28) (30) and $BO_{12}EO_{260}BO_{12}$ (N_w= 29)[18]. In this regard, it is worth mentioning that $BO_mEO_nBO_m$ copolymers possessing EO < 300 units exhibit an increase in $N_w$as their hydrophobic block length increases as observed for $BO_5EO_{91}BO_5$, $BO_6EO_{46}BO_6$ (30), $BO_7EO_{40}BO_7$ [18], $BO_{10}EO_{271}BO_{10}$ and $BO_{12}EO_{270}BO_{12}$,[30] for example. Conversely, $BO_mEO_nBO_m$ copolymers with EO >300 units decrease their N_w values as the BO block length increases as, for example, from 18 to 9 for $BO_{14}EO_{378}BO_{14}$ and $BO_{21}EO_{385}BO_{21}$, or from 8 to 7 for $BO_{10}EO_{410}BO_{10}$ and $BO_{20}EO_{411}BO_{20}$, respectively. This trend is a consequence of steric restrictions of the lengthy EO corona to efficiently pack more hydrophobic chains inside the micellar core nuclei.[17]

Table 2. Micellar data obtained from DLS experiments at 10 and 25ºC for copolymers $BO_8EO_{90}BO_8$ and $BO_{20}EO_{411}BO_{20}$.

Polymer	T (ºC)	$10^5 M_W$ (g/mol)	r_h (nm)	N_w	$10^{-4}A_2$ (mol·cm^{3}g^{-2})
$BO_8EO_{90}BO_8$	10	1.4	9.7	25	-8.3
	25	2.1	13.0	38	-19.7
$BO_{20}EO_{411}BO_{20}$	10	2.4	10.6	11	-10.7
	25	3.8	18.9	17	-60.2

On the other hand, Figure 4a shows the dependence of N_w on BO-block length for different $BO_mEO_nBO_m$ reported so far[17]. Values of N_w were adjusted for differences in n (the EO block length) using the scaling exponent $N_w \sim (n')^{1.07}$, where n' ($n' = n - n_{crit}$, $n_{crit} = 4$ is the effective hydrophobic block length, that is, the minimum hydrophobic block length in reverse $BO_mEO_nBO_m$ for micellization) is the effective hydrophobic block length. The line through the data points of $\log(N_w/n'^{1.07})$ against log (m) has a slope of -0.84. Attwood *et al.* previously obtained an exponent of -0.63,[17] whilst Föster *et al.* derived an exponent of -0.71 for short C_nEO_m copolymers with n = 8-16 and m = 4-23.[31] The difference may arise from introducing $BO_mEO_nBO_m$ copolymers with extremely lengthy EO blocks (EO > 375 units) and long BO blocks (BO > 14) in Figure 4a, which possess relatively low aggregation numbers due to their very long chains. On the other hand, Figure 4b effectively verified that data points plotted as $\log(N_w/m^{0.84})$ against $\log(n')$ do indeed fit satisfactorily to a straigth line of slope 1.0 with evident correspondence with scaling exponents of N_w as a function of the EO block length (ca. 1.07) derived from diblock and non-bridging triblock copolymers.

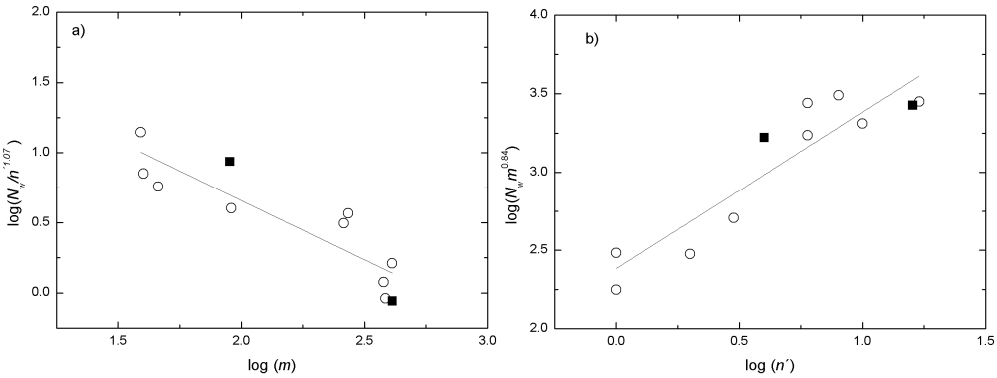

Figure 4. a) Dependence of the association number on a) EO-block length, *m,* and b) effective hydrophobic block length, *n´*. Association numbers are corrected for variation in hydrophobic and hydrophilic block lengths, respectively. (■) denote the copolymers studied.

Rheological behaviour

Tube inversion

Tube inversion was used to obtain a preliminary definition of the mobile-immobile regions of the phase diagram of each copolymer. For both polymers the mobile region (sol) transforms progressively into a viscous fluid and, then, to a gel as the concentration increases. For $BO_8EO_{90}BO_8$ a mobile viscous fluid was present up to a concentration of 6 wt.% whilst an immobile gel was formed above (Figure 5). The gel phase progressively converts into a very viscous fluid, resembling a high temperature boundary, in the temperature range 40 to 70 ºC depending on concentration: the higher the concentration the larger the boundary temperature was. In the case of copolymer $BO_{20}EO_{411}BO_{20,}$ a mobile more or less viscous fluid is present up to 8 wt.%, whilst an immobile transparent gel is formed above such value within a determined temperature range, which is broader as the copolymer concentration increases. At 12 wt.%, the gel phase of the present copolymer is present along the whole temperature range analyzed. Comparison of phase transitions of $BO_nEO_mBO_n$ copolymers with lengthy EO blocks (EO > 350 units) showed that the transition point from sole to soft gel largely depends on the EO block length at temperatures below room temperature, whilst the change from soft-gel to hard gel is dominated by the BO/EO ratio, that is, the most hydrophobic the copolymer is, the gel phase appears at lower concentrations and temperatures.[29]

To perfectly define the boundaries of the phase diagrams and to further characterize the flow behaviour of semi-dilute and concentrated copolymer solution, rheometry measurements were also performed.

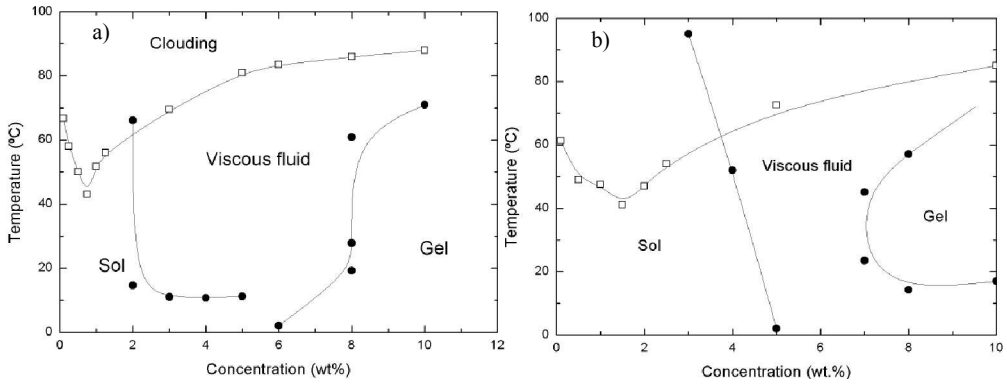

Figure 5. Phase diagrams depicted by using tube inversion and rheometry data from temperature scan for a) $BO_8EO_{90}BO_8$, and b) $BO_{20}EO_{411}BO_{20}$. (□) denote clouding boundaries obtained UV-Vis, whereas (●) are experimental points measured by rheometry. Lines were only drawn to guide the eye.

Concentration and temperature dependence of storage and loss moduli

Oscillatory tests were performed in order to determine the linear viscoelastic region in which oscillatory shear measurements need to be performed ensuring, at the same time, that the system is frequency-dependent (see Figure S1). G'' values were consistently smaller than the G' ones for both copolymers (not shown). A linear region in which the G' value was almost independent of strain was observed. In addition, for both copolymers G' and G'' increases as copolymer concentration does being G' larger for $BO_8EO_{90}BO_8$ than for $BO_{20}EO_{411}BO_{20}$; however, it is observed that while for $BO_8EO_{90}BO_8$ the linear viscoelastic region becomes wider as the concentration increases, for copolymer $BO_{20}EO_{411}BO_{20}$ the opposite behaviour is found. This different behaviour results from differences in packing and flow behaviour between both copolymers. In particular, as observed from DLS data, copolymer $BO_8EO_{90}BO_8$ would form smaller free micelles and relatively strong bridging micelles; these would involve the formation of a more compact, stronger and flexible nanostructure (for example, reflected in a sol-hard gel transition around a copolymer concentration of 5-6 wt.%, see below for further details) which would help to explain the increase of the linear viscoelastic region with concentration. By contrast, copolymer $BO_{20}EO_{411}BO_{20}$ would form larger sized micelles which would lead to less compact structures as the copolymer concentration increases (reflected, for example, in the formation of gel structures at larger concentration compared to copolymer $BO_8EO_{90}BO_8$, see below) generating weaker nanostructures; as an additional consequence, a decrease of the lineal viscoelastic region with the copolymer concentration occurs.

Once determined the linear viscoelastic region, temperature scans in the range 1-90 ºC of log (G') at $f = 1$ Hz for copolymers $BO_8EO_{90}BO_8$ and $BO_{20}EO_{411}BO_{20}$ were performed. The dependence of G' on concentration and temperature is provided by the examples shown in Figure 6. At 1 wt.%, copolymer samples are unstructured fluids (sols, with $G'<10$ Pa and $G''>G'$). At 2 wt.% copolymer $BO_8EO_{90}BO_8$ was a viscous complex fluid characterized by $10 < G' < 1000$ Pa and $G' > G''$ (*i.e.* a soft gel adopting Hvidt´s *et al.* notation),[32] in the temperature range 16 to 63ºC, and it became a sol below and above such temperature interval (Figure 6a). In particular, the observed decrease in G'

at high temperatures and, thus, the transition from a viscous fluid to a sol can be associated with a worsening solvent environment compressing the EO-block corona. In the concentration range from 3 to 5 wt.%, this copolymer was a viscous fluid in the whole temperature range analyzed above 5 ºC. At 6 wt.% copolymer $BO_8EO_{90}BO_8$ became a gel (arbitrarily defined by $G'>G''$ and $G'>$ 1000 Pa at f = 1 Hz, a hard gel adopting Hvidt´s et al. notation) within the temperature range 5-20 ºC and above it becomes a viscous fluid. The gel region subsequently expands within a broader temperature range as the copolymer concentration increases (from 0 to 27ºC, at 8 wt.% and until 70 ºC at 10 wt.%); above the upper limit temperature the copolymers becomes a soft gel. Hence, despite their reverse structure, copolymer $BO_8EO_{90}BO_8$ displayed a behaviour similar to diblock EO_nBO_m and triblock $EO_nBO_mEO_n$ copolymers, in which micellar packing determines the moduli behaviour as the polymer concentration increases.

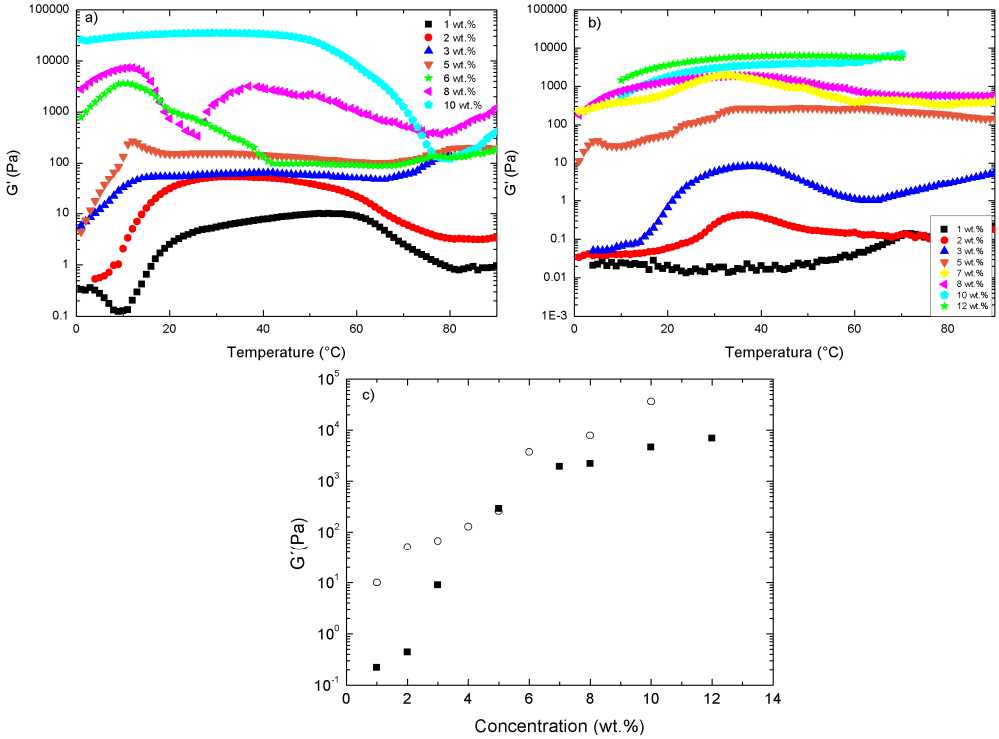

Figure 6. Temperature scans in the range 1-90 ºC of G' at f = 1 Hz for copolymers a) $BO_8EO_{90}BO_8$ and b) $BO_{20}EO_{411}BO_{20}$ at different concentrations. c) Plots of G'_{max} against concentration for copolymers (○)$BO_8EO_{90}BO_8$ and (■) $BO_{20}EO_{411}BO_{20}$.

Despite possessing longer hydrophobic and hydrophilic blocks, the larger EO/BO ratio and the existence of bridging which may difficult effective cubic packing makes copolymer $BO_{20}EO_{411}BO_{20}$ to remain in a sol state up to a concentration of 3 wt.% (Figure 6b). At 4 wt.% it already became a viscous fluid between ca. 30 and 50ºC and 5 and 6 wt.% in the whole temperature range. At 7 and 8 wt.% this copolymer is a gel between 24-45ºC and 14-57ºC, respectively and a viscous fluid in the remaining temperature interval. At 10 wt.%, the copolymer is a gel above 20 ºC and in the whole temperature range at 12 wt.%. All the above data allowed a more exact definition of the phase diagram, as shown in Figure 5. On the other hand, maximum values of $G'(T)$, G'_{max} of copolymer $BO_{20}EO_{411}BO_{20}$ are

similar to those of structurally related copolymers with EO blocks ~400 units such as $BO_{21}EO_{385}BO_{21}$ and $BO_{14}EO_{378}BO_{14}$; in addition, copolymer $BO_8EO_{90}BO_8$ possesses G'_{max} values larger than the latter copolymers despite having much lower BO and EO units as a consequence of a better cubic packing of micelles with shorter solvated EO coronas. Despite de observed differences, both $BO_8EO_{90}BO_8$ and $BO_{20}EO_{411}BO_{20}$ copolymers G' values increased markedly with concentration, with a predominant elastic behavior ($G' > G''$) in most of the temperature and concentration ranges analyzed, as occurred for other reverse $BO_nEO_mBO_n$ copolymers with lengthy EO blocks (Figure S2).

As discussed elsewhere[33] for aqueous micellar gels of copoly(oxyalkylene)s of different block architectures, the onset of gelation and the associated increase in G' with T at low temperatures for copolymer $BO_{20}EO_{411}BO_{20}$ is associated with an increase in the extent of micellization and, in the present case, with the extent of bridging. This is in contrast with the behavior observed for $BO_8EO_{90}BO_8$ whose G' values in the gel region (at 10 wt.%) are fairly constant until relatively high temperatures (> 70 ºC) at which then decrease. This observed decrease in G' at high temperatures can be associated with a worsening solvent environment compressing the EO-block corona and, thereby, with a decrease in the effective micellar volume fraction. This viscous fluid after the immobile gel phase has been shown to be composed by small micellar domains with the same structure as the gel phase as observed by SAXS and SANS;[34] hence, it can be characterized as a defective cubic structure, as previously observed for related EO_mBO_n and $EO_mBO_nEO_m$ copolymers.[33]

Frequency scans

Effects of changes in the extent of micellar bridging and packing are apparent in the different mechanical responses of the system to the applied frequency. Hence, the frequency dependence of the modulus was determined for solutions of copolymers $BO_8EO_{90}BO_8$ and $BO_{20}EO_{411}BO_{20}$ in the concentration range 1-10 wt.%. For example, Figure 8a shows an 1 wt.% solution for copolymers $BO_8EO_{90}BO_8$ and $BO_{20}EO_{411}BO_{20}$ at 10ºC, with values of G'' exceeding those of G' over most accessible frequency range, except at high frequencies, where a moduli crossover occurs from which a relaxation time t = 0.90 and 0.35 s, respectively, could be determined. The behavior can be approximated to that of a Maxwell element:

$$G' = (G_\infty \tau^2 \omega^2)/(1 + \tau^2 \omega^2)$$
$$G'' = (G_\infty \tau \omega)/(1 + \tau^2 \omega^2) \quad (3)$$

where G_∞ is the plateau value of G' at high frequency, τ is the relaxation time, and $\omega = 2\pi f$ (f = frequency in Hz). At all temperatures investigated, the slopes of the best straight lines through the data points were near to values of 2 (*logG'*) and 1 (*logG''*) which are expected when $\omega\tau << 1$, *i.e.* typical of a Newtonian fluid.

For copolymer $BO_{20}EO_{411}BO_{20}$ G'' is consistently larger than G' in the whole frequency range analysed in the concentration range 2-4 wt.% at temperatures below 50 ºC except at very frequencies (f > 10 Hz) where a moduli crossover takes place. At larger temperatures, the moduli crossover can be observed at much lower frequencies corresponding to a Maxwell fluid showing, at most, localized cubic order (Figure 8b).[33] This effect must be a consequence of the attraction of micelles at temperatures at which water is a poor solvent for micelles, and favored by micellar bridging too. A similar behavior can be observed at larger copolymer $BO_{20}EO_{411}BO_{20}$concentrations (5-7 wt.%) and for copolymer for copolymer $BO_8EO_{90}BO_8$ in the concentration range 2-5 wt.% but only at temperatures below room temperature (Figure 8c). Then, as the concentration is further increase for both copolymers (> 8 wt.% and 6 wt.% for $BO_{20}EO_{411}BO_{20}$ and $BO_8EO_{90}BO_8$, respectively) an immobile gel with relatively high G' values (> 1 kPa) existed typically below 70 ºC depending on copolymer type and concentration, as commented previously. Above such temperature threshold, a viscous fluid was observed (Figure 8d). This type of viscous fluid at temperatures and concentrations relatively near the gel boundary can be assigned as defective versions of cubic packed gels as mentioned previously; they are characterized by a constant value of G', the shallow minimum in G'', and both moduli do not show a crossover point in the measured frequency range as observed in Figure 8d. Nevertheless, the G' values for the viscous fluid are much lower compared to those of a pure gel phase, which well exceeded 1 kPa and possessed the characteristic features of immobile gels constituted by cubic packing of spherical micelles completely independent on temperature and frequency.[35] The plateau behavior of G' and the minimum in G'' have been also observed for colloidal hard spheres near the glass-fluid transition,[36] and is also characteristic of the cubic phase in block copolymer melts[37]. The frequency-independent regime took place at lower concentrations for copolymer $BO_8EO_{90}BO_8$ than for $BO_{20}EO_{411}BO_{20}$ due to its larger BO/EO ratio, which favored micellization.

Plots of $G'$and G''*vs* frequency presented in Figure 8 show a wide variety of characteristics from purely viscous to highly elastic fluids. The observed behaviours seems to confirm the formation of a dynamic network for both copolymers, but specially for $BO_{20}EO_{411}BO_{20}$, which becomes more and more robust as the concentration is increased, as observed for other $BO_mEO_nBO_m$ copolymers with very lengthy EO blocks as $BO_{12}EO_{114}BO_{12}$[13], $BO_{10}EO_{227}BO_{10}$[26], $BO_{12}EO_{227}BO_{12}$,[28] $BO_{10}EO_{410}BO_{10}$[11], $BO_{21}EO_{385}BO_{21}$ and $BO_{14}EO_{378}BO_{14}$.[27] The existence of slow relaxation processes as the copolymer concentration increases also seems to corroborate this point. For $BO_8EO_{90}BO_8$ micelle packing as effective hard spheres in the gel phase becomes the predominant response at much lower concentrations than for copolymer $BO_{20}EO_{411}BO_{20,}$ which agrees with that previously mentioned.

On the other hand, copolymer $BO_{20}EO_{411}BO_{20}$ showed rather different behavior to that observed for other structurally related copolymer, $BO_{10}EO_{410}BO_{10}$. For this copolymer typical values of G'' exceed those of G' over a similar accessible frequency range, as also observed for other classical associative thickeners.[38] Despite the similar EO length and larger BO blocks compared with $BO_{10}EO_{410}BO_{10}$, the larger polydispersity of $BO_{20}EO_{411}BO_{20}$ (as also occurred for copolymers $BO_{14}EO_{378}BO_{14}$ and $BO_{21}EO_{385}BO_{21}$) can broad the Poisson distribution of BO block-lengths (assuming ideal polymerization),[39] which involves a wider temperature range for micellization. Hence, this

copolymer effectively behaves as having lower effective BO block lengths with a behavior more related to that observed to $BO_{12}EO_{114}BO_{12}$, $BO_{10}EO_{227}BO_{10}$ or $BO_{10}EO_{227}BO_{10}$ copolymers. Also, both $BO_8EO_{90}BO_8$ and $BO_{20}EO_{411}BO_{20}$ do not behave as classical colloidal suspensions interacting through weak short-range attractive forces, that is, *G´* being frequency-independent and increasing with concentration, and *G´´* being concentration-independent and increasing linearly with frequency. All these facts allow to scale the moduli against frequency to give smooth master curves,[40] which allows to gain access to sample´s behaviour under frequencies that are not accessible using common instrumentation (see below).

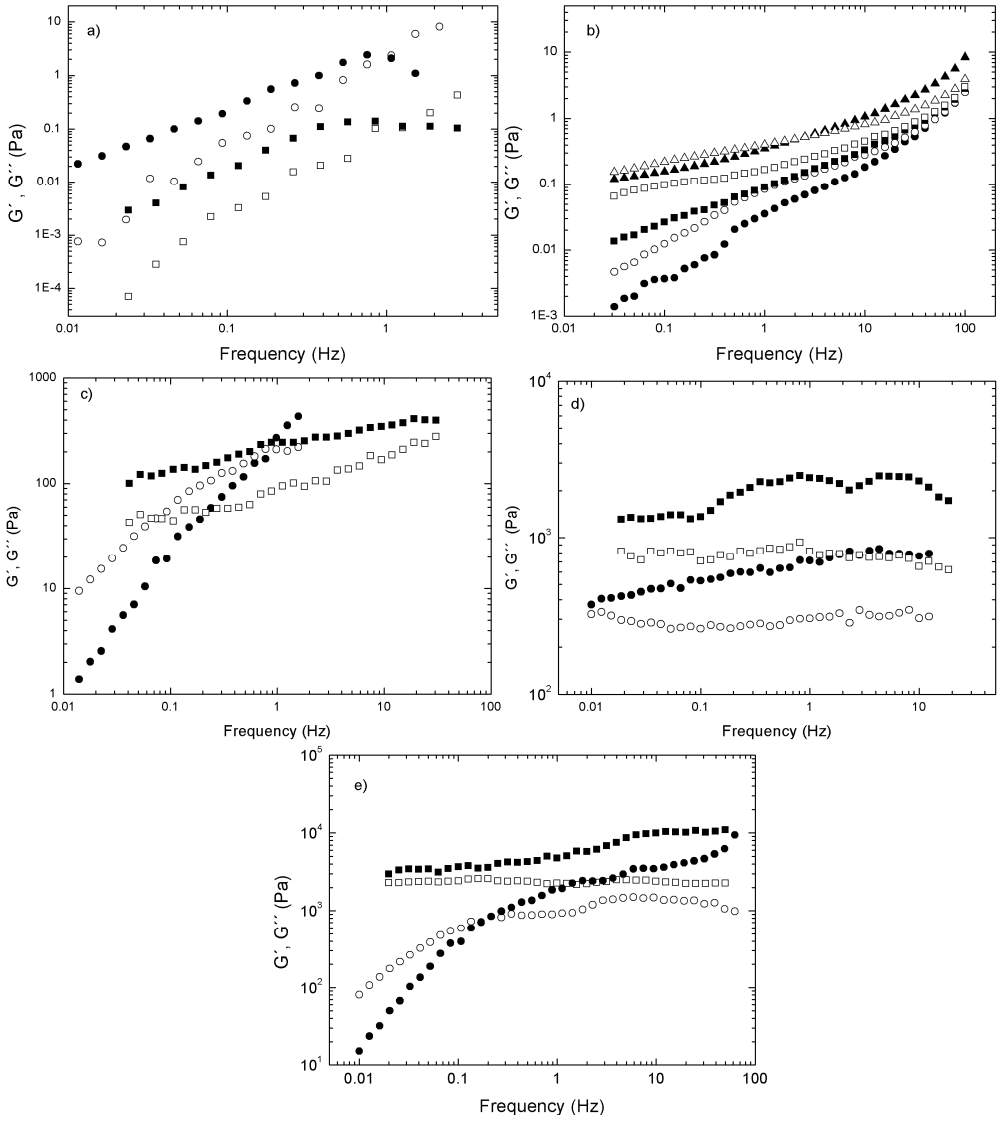

Figure 8. Frequency scans for the present copolymers at different concentrations and temperatures: a) $BO_8EO_{90}BO_8$ (●,○) and $BO_{20}EO_{411}BO_{20}$ (■,□) at 2 wt.% and 10 ºC; b) $BO_{20}EO_{411}BO_{20}$ copolymer at 3 wt. % and (●,○) 10 ºC, (■,□) 20 ºC, and (▲,△) 60 ºC; c) $BO_8EO_{90}BO_8$ copolymer at 5 wt. % and (●,○) 10 ºC and (■,□) 40 ºC; d) $BO_8EO_{90}BO_8$ copolymer at 8 wt.% and (●,○) 30 ºC and (■,□) 50 ºC; $BO_{20}EO_{411}BO_{20}$ copolymer at 12 wt. % at (●,○) 10 ºC and (■,□) 40 ºC. Closed symbols denote *G´* whilst open ones correspond to *G´´*.

Scaling of rheological response

The construction of a master curve through the time-temperature superposition of the measured moduli was performed in order to facilitate comparison of the frequency response at different temperatures of copolymers $BO_8EO_{90}BO_8$ and $BO_{20}EO_{411}BO_{20}$. The moduli and the frequencies for each data set were independently scaled by factors a_T and b_T, respectively, to obtain a superposition of G' and G''. The temperature dependence of the moduli was explored for the copolymers in the gel region. Figure 9a and Figure S3 show the superposition achieved at 8 wt. % and 12 wt. % for copolymers $BO_8EO_{90}BO_8$ and $BO_{20}EO_{411}BO_{20}$, respectively. The data suggest that there are no changes in the nature of the dynamic mechanical response in the gel phase as a function of temperature in the range 10-50 ºC. As already discussed, higher temperatures worsen the solvent environment and progressively compress the micellar corona. The shrinkage of the micellar corona will lead to defects in micellar packing and the bridged network, which may well change the scaling of the viscoelastic behaviour with frequency within the hard gel phase.

The Arrhenius plot of $-log(a_T)$ against $1/T$ (Figure 9b and Figure S4), which has a slope equivalent to a plot of log(relaxation rate) against $1/T$, gave activation energy values (the energy related to the relaxation mechanism in crosslinking or bonding processes) through the application of the Williams-Landel-Ferry equation[41]

$$\log a_T = -C_1(T-T_r)/(C_2 + (T-T_r)) \quad (4)$$

where T is the temperature, T_r is the reference temperature to construct the compliance master curve, and C_1 and C_2 are empirical constants to fit the values of the superposition. Therefore, the activation energy, E_a, can be derived as

$$E_a = 2.303\, R\, C_1\, C_2\, T^2/(C_2 + T - T_r)^2 \quad (5)$$

Activation energies of E_a = -11 and -41 kJ/mol were obtained for copolymers $BO_8EO_{90}BO_8$ and $BO_{20}EO_{411}BO_{20}$, respectively, as an average value over all components of the copolymer solutions. The negative values imply that the relaxation time increases as temperature rises, which is in agreement with the progressive hardening of the gel in the temperature range analyzed.[11] As can be seen in Figure 9b, the obtained slope for copolymer $BO_{20}EO_{411}BO_{20}$ (and hence, activation energies) is rather to other $BO_nEO_mBO_n$ copolymers having EO bock lengths > 350 units, as for example, $BO_{10}EO_{410}BO_{10}$ (E_a = -40 kJ/mol) or $BO_{21}EO_{385}BO_{21}$ (E_a = -50 kJ/mol).[11,27] In fact, there is a slight increase in the slope net value obtained for the BEB block copolymers as the BO/EO ratio increases.

Also, the negative activation energy values indicate that both the disengagement of chain ends from micelles (a positive contribution) and micellization (a negative one) can contribute in contrast to alkyl-ended copolymer solutions, where only disengagement is important provided that their extent of micellization is low over the temperature range of interest and, hence, positive activation energies are obtained.[42,43] This behaviour is

confirmed when analyzing the dependence of storage modulus with temperature by plotting $1/b_T$ against T (see Figure 9c). Copolymer $BO_8EO_{90}BO_8$ at 8 wt. % exhibits an important decrease of $1/b_T$ (or storage modulus) with temperature. This decrease is much greater in the low temperature range in agreement with the progressive shrinkage of the cubic mesoscopic structure of packed micelles and the increased tendency as temperature is increased for the copolymers to loop in a single micelle rather than to bridge between micelles.[43] Conversely, for copolymer $BO_{20}EO_{411}BO_{20}$ a slight increase of $1/b_T$ against T can be observed, which points to an increase in the high-frequency storage modulus in the temperature interval analyzed compatible with an increase in the extent of micellization and, then, of bridging. This temperature dependence is greater than that predicted by the kinetic theory of elasticity for a fully formed network.

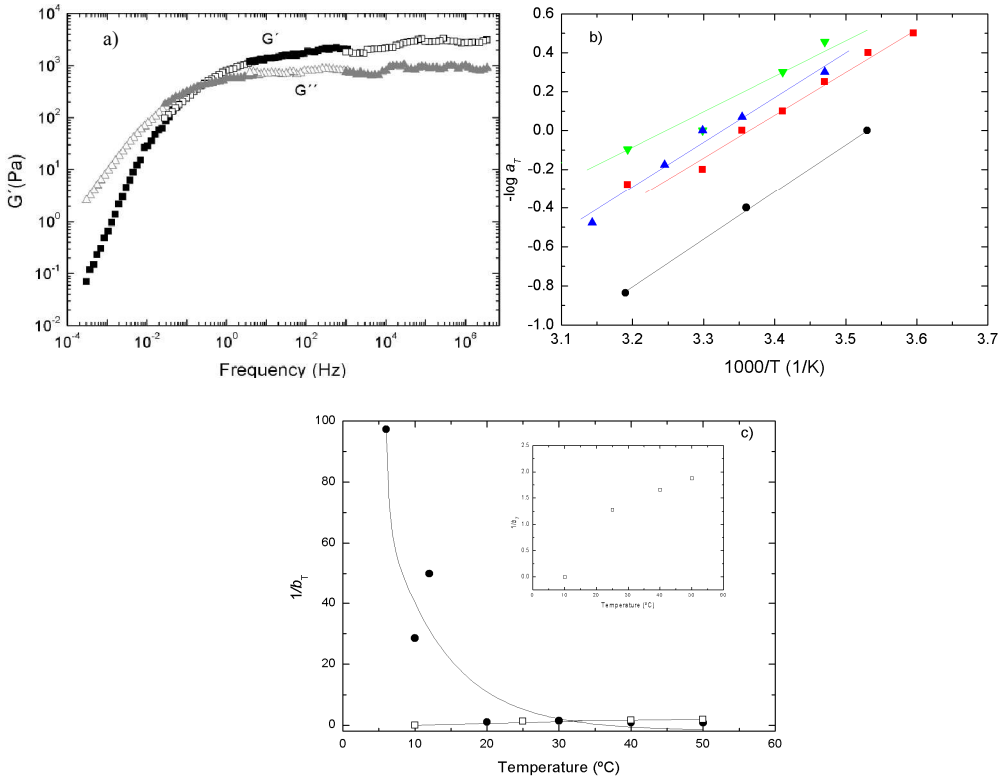

Figure 9. a) Master curve plots obtained for copolymer $BO_8EO_{90}BO_8$ at 8 wt.% (reference temperature T_r = 10ºC). b) Arrhenius plot for copolymer (●) $BO_{20}EO_{411}BO_{20}$, (■) $BO_{10}EO_{410}BO_{10}$, (▲) $BO_{21}EO_{385}BO_{21}$, and (▼) $BO_{14}EO_{378}BO_{14}$ Concentration for $BO_{20}EO_{411}BO_{20}$, $BO_{21}EO_{385}BO_{21}$, and $BO_{14}EO_{378}BO_{14}$ is 12 wt. % whilst for $BO_{10}EO_{410}BO_{10}$ is 15 wt.%. c) Temperature dependence of $1/b_T$ for copolymers (●) $BO_8EO_{90}BO_8$ and (□) $BO_{20}EO_{411}BO_{20}$ (see also inset) at 8 and 12 wt.%, respectively.

Conclusions

In summary, the present $BO_8EO_{90}BO_8$ and $BO_{20}EO_{411}BO_{20}$ copolymers form swollen flower-like micelles with sizes ranging from ca. 13 to 30 nm. Copolymer $BO_8EO_{90}BO_8$ can form individual micelles in very dilute solutions whilst $BO_{20}EO_{411}BO_{20}$ already display a secondary population at sizes ca. 200-300, which represents interconnected micelles by bridging as confirmed by AFM images. At slightly larger concentrations, these micellar clusters are

already observed for both copolymers and even for $BO_{20}EO_{411}BO_{20}$ a third population with sizes ca. 3000-4000 nm is detected which would correspond to the aggregation of several micellar bridged clusters. As a result of their long BO blocks and extremely lengthy EO ones, these two copolymers exhibited very rich phase behaviours. This could be modulated from an unstructured fluid to a viscoelastic one to a fully developed gel by changing the solution temperature and concentration. In particular, bridging could be observe by the appearance of slow relaxation modes at relatively low polymer concentrations as denoted form the frequency scans, specially for copolymer $BO_{20}EO_{411}BO_{20}$ thanks to their lengthy EO blocks and longer BO ones, which favoured a much larger exclusion volume and intermicellar attraction while reaching a less efficient packing of micelles. As the concentration increases the dynamic network becomes more robust as the concentration, which impeded to fit their behaviour to that of Maxwell fluid. At this respect and confirming this view, copolymer $BO_8EO_{90}BO_8$ displays a more classical behaviour of packed mesoscopic cubic structures in the gel phase at much lower concentrations than $BO_{20}EO_{411}BO_{20}$. The negative values of the activation energy for the relaxation processes derived from master curves might involve both the disengagement of chain ends from micelles (a positive contribution) and micellization (a negative one), with evident predominance of the latter.

Acknowledgements

Authors thank Ministerio de Economía y Competitividad (MINECO) and Xunta de Galicia for research projects MAT2013-40971-R and EM2013-046, respectively. S.B. also thanks MINECO for her Ramón y Cajal fellowship.

References

1 D.N. Schulz, J.E. Glass, *Polymer as Rheology Modifiers. ACS Symp. Ser.* Eds. American Chemical Society, Washington DC, 1991, **462**.

2 E.E. Glass, *Water -soluble Polymers: Beauty with Performance.* Ed. American Chemical Society, Washington DC, 1986, **213**.

3 M.A. Winnik, A. Yekta, *Curr. Opin. Colloid Interface Sci.* 1997, **2**, 424-436.

4 S. Francois, S. Maitre, M. Rawiso, D. Sarazin, G. Beinert, F. Isel, *Colloids Surfaces A*, 1996, **112**, 251-265.

5 E. Beaudoin, O.V. Borisov, A. Lapp,J. Francois, *Macromol. Symp.* 2002, **191**, 89-98.

6 D. Mistry, T. Annable, C. Booth, *ACS Abstr.* 1999, *218*, 41.

7 T. Annable, R. Buscall, R. Ettelaie, D. Whittlestone, *J. Rheol.* 1993, **37**, 695-726.

8 K. Mortensen, W. Brown, E. Jørgensen, *Macromolecules* 1994, **27**, 5654-5666.

9 H. Altinok, G.-E. Yu, S.K. Nixon, P.A. Gorry, D. Attwood, C. Booth, *Langmuir* 1997, **13**, 5837-5848.

10 A. Cambón, M. Alatorre-Meda, J. Juárez, A. Topete, D. Mistry, D. Attwood, S. Barbosa, P. Taboada, V. Mosquera, *J. Colloid Interface Sci.* 2011, **361**, 154-158.

11 Mistry, D.; Annable, T.; Yuan, X.-F.; Booth, C. *Langmuir* 2006, **22**, 2986-2992.

12 V. Castelletto, I.W. Hamley, X.-F. Yuan, A. Kelarakis, C. Booth, *Soft Matter* 2005, **1**, 138-145.

13 A. Kelarakis, X.-F. Yuan, S.-M. Mai, Y.-W. Yang, C. Booth C. *Phys. Chem. Chem. Phys.* 2003, **5**, 2628-2634.

14 S.-M. Mai, S. Ludhera, F. Heatley, D. Attwood, C. Booth, *J. Chem. Soc. Faraday Trans.* 1998, **94**, 567-572.

15 N.M.P.S. Ricardo, S.B. Honorato, Z. Yang, V. Castelletto, I. W. Hamley, X.-F. Yuan, D. Attwood, C. Booth, *Langmuir* 2004, **20**, 4272-4278.

16 G.-E. Yu, A. J. Masters, F. Heatley, C. Booth, T.G. Blease, *Macromol. Chem. Phy.* 1994, **195**, 1517-1538.

17 C. Booth, D. Attwood, C. Price, C. *Phys. Chem. Chem. Phys.* 2006, **8**, 3612-3622.

18 Z. Zhou, Y.-W. Yang, C. Booth, B. Chu, *Macromolecules* 1996, **29**, 8357-8361.

19 A. Cambón, A Rey-Rico, D. Mistry, J. Brea, M.I. Loza, D. Attwood, S. Barbosa, C. Alvarez-Lorenzo, A. Concheiro, P. Taboada, V. Mosquera, *Int. J. Pharm.* 2013, **445**, 47-57.

20 M.E.N.P. Ribeiro, I.M. Cavalcante, N.M.P.S. Ricardo, S.-M- Mai, D. Attwood, S.G. Yeates, C. Booth, *Int. J. Pharm.* 2009, **369**, 196-198.

21 D. Attwood, C. Booth, S.G. Yeates, C. Chaibundit, N.M.P.S. Ricardo, *Int. J. Pharm.* 2007, **345**, 35-41.

22 A. Cambón, J. Brea, M.I. Loza, C. Alvarez-Lorenzo, A. Concheiro, S. Barbosa, P. Taboada, M. Mosquera, *Mol. Pharm.* 2013, **10**, 3232-3241.

23 Y.-W- Yang, Z. Yang, Z.-K. Zhou, D. Attwood, C. Booth, *Macromolecules* 1996, **29**, 670-680.

24 S.W. Provencher, *Die Makromol. Chem.* 1979, **180**, 201-209.

25 T. Liu, V.M. Nace, B. Chu, *J. Phys. Chem. B* 1997, **101**, 8074-8078.

26 A. Kelarakis, V. Havredaki, X.-F. Yuan, C. Chaibundit, C. Booth, *Macromol. Chem. Phys.* 2006, **207**, 903-909.

27 A. Cambón, E. Figueroa-Ochoa, J. Juárez, E. Villar-Alvarez, A. Pardo, S. Barbosa, J.F.A. Soltero, P. Taboada, V. Mosquera, *J. Phys. Chem. B*. 2014, **118**, 5258-5269.

28 A. Kelarakis, X.-T. Ming, X.-F. Yuan, C. Booth, *Langmuir* 2004, **20**, 2036-2038.

29 A. Cambón, S. Barbosa, A. Rey-Rico, E.B. Figueroa-Ochoa, J.F.A. Soltero, S.G. Yeates, C. Alvarez-Lorenzo, A. Concheiro, P. Taboada, V. Mosquera, *J. Colloid Interface Sci.* 2012, **387**, 275-284.

30 T. Liu, Z. Zhou, C. Wu, V.M. Nace, B. Chu, *J. Phys. Chem. B* 1998, **102**, 2875-2882.

31 S. Föster, M. Zisenis, E. Wenz, M. Antonietti, *J. Chem. Phys.* 1996, **104**, 9956-9970.

32 S. Hvidt, E.B. Joergensen, W. Brown, K. Schillen, *J. Phys. Chem.* 1994, **98**, 12320-12328.

33 I.W. Hamley, S.-M. Mai, A.J. Ryan, P.A. Fairclough, C. Booth, *Phys. Chem. Chem. Phys.* 2001, **3**, 2972-2980.

34 R.K. Prud'homme, G. Wu, D.K. Schneider, *Langmuir* 1996, **12**, 4651-4659.

35 J. Juárez, P. Taboada, M.A. Aldez, V. Mosquera, *Langmuir* 2008, **24**, 7107-7116.

36 T.G. Mason, D.A. Weitz, *Phys. Rev. Lett.* 1995, **75**, 2770-2773.

37 J. Zhao, B. Majumdar, M.F. Schulz, F.S. Bates, *Macromolecules* 1996, **29**, 1204-1215.

38 T. Annable, R. Buscall, R. Ettelaie, *Colloids Surfaces A* 1996, **112**, 97-116.

39 P.J. Flory, *Principles of Polymer Chemistry.* Cornell University Press, Ithaca, 1953.

40 V. Trappe, D.A. Weitz, *Phys. Rev. Lett.* 2000, **85**, 449-452.

41 J.D. Ferry, *Viscoelastic Properties of Polymers*, Wiley, London, 1980.

42 P. Alexandridis, B. Lindman, *Amphiphilic Block Copolymers. Self-Assembly and Applications.* Elsevier, Amsterdam, 2000.

43 D. Mistry, Ph.D. Thesis, University of Manchester, Manchester, UK. 2000.

TOC FIGURE

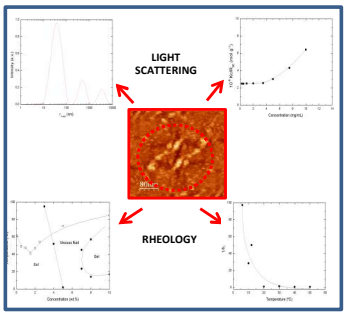

REVERSE ARCHITECTURE OF $BO_nEO_mBO_n$ BLOCK COPOLYMERS ENABLES THE FORMATION OF MICELLAR CLUSTERS AND VISCOUS GELS AT LOW CONCENTRATIONS BY CHAIN BRIDGING